Magnetic Nanoparticles

DOI: 10.1002/anie.200901570

Unusual Magnetic Properties of Size-Controlled Iron Oxide Nanoparticles Grown in a Nanoporous Matrix with Tunable Pores**

*Sher Alam, Chokkalingam Anand, Katsuhiko Ariga, Toshiyuki Mori, and Ajayan Vinu**

Magnetic iron oxide nanoparticles have been much investigated because of their promising applications in data storage, electronic and biomedical devices, and magnetic carriers for drug delivery.[1,2] However, many of these applications require Fe_2O_3 nanoparticles with controllable sizes, as they exhibit interesting magnetic properties. The fabrication of such nanoparticles is always a challenging task. Consequently, several synthetic approaches, including heating, hot injection, sonochemistry, and thermal decomposition of organometallic compounds, have been employed for the fabrication of Fe_2O_3 nanoparticles with uniform size and shape.[3] However, most of the synthetic approaches generate agglomerated Fe_2O_3 nanoparticles with large sizes and irregular shapes. These nanoparticles have drawbacks such as low magnetic moments. An interesting way to finely control the particle size and shape is to encapsulate magnetic particles inside a porous inorganic template matrix[4] with defined pore size and shape.

Herein, we demonstrate the first nanosieve approach for the fabrication of magnetic Fe_2O_3 nanoparticles with controllable sizes inside a nanoporous confined matrix of hexagonally ordered silica materials with tunable pore diameters. The preparation of this matrix using a high-temperature hydrothermal approach was recently reported by us.[5] We further demonstrate that the sizes and the magnetic properties of the nanoparticles can easily be controlled by simply tuning the pore size of the nanoporous silica matrix. The loading of a metal source in the nanoporous matrix also plays a critical role in controlling the particle size in the confined nanoporous matrix and significantly affects the magnetic properties of the particles.

Mesoporous SBA-15 supports with various pore diameters were prepared by a hydrothermal technique following our previous reported procedure[5] (see Tables 1S and 2S in the Supporting Information for the textural parameters and the conditions for synthesis of the samples). The Fe_2O_3 nanoparticles in the supports were prepared by the wet impregnation method (see the Experimental Section). The samples were denoted as XF-SBA-15-Z where X and Z are the weight % of the Fe and the temperature used for the synthesis of SBA-15, respectively, and F denotes Fe_2O_3.

The representative HRTEM image and the related HRTEM histogram of 30F-SBA-15-130 are shown in Figure 1a and 1b, respectively. The image clearly shows that the Fe_2O_3 nanoparticles have uniform size and shape. It is also clear that the nanoparticles are encapsulated inside the linear array of SBA-15-130 pores, which are arranged in regular intervals, thus confirming that the ordered pores indeed control the size and shape of the Fe_2O_3 nanoparticles (Figure 1a inset). It is interesting to note that the diameter of the Fe_2O_3 particles grown inside the SBA-15 nanochannels is between 6.5 and 9.0 nm, which is quite similar to the pore size of the SBA-15 supports and significantly smaller than that of the particles made without SBA-15 matrix (Tables 1S, 2S and Figures 1S, 2S in the Supporting Information). Interestingly, the size of the Fe_2O_3 nanoparticles increases with the pore size of SBA-15. The powder XRD diffraction patterns of 30F-SBA-15-130 and parent SBA-15-100 are compared in Figure 1b. Both samples show a sharp peak at lower angles, and several higher-order peaks, which can be indexed to the (100), (110), and (200) reflections of the hexagonal space group p6mm, and are indicative of hexagonally ordered pore structure. However, the intensity of the peaks at lower angles decreases significantly as the loading of Fe_2O_3 nanoparticles inside the mesochannels of SBA-15 is increased (Figure 3S in the Supporting Information). It is unlikely that the large difference in the intensity of the (100) peak before and after the Fe_2O_3 immobilization arises from damage to the structure, but rather from a larger contrast in density between the silica walls and the open pores relative to that between the silica walls and iron oxide inside the porous channels. The wide-angle XRD pattern of 30F-SBA-15-130 shows several higher-angle peaks, which are quite similar to those of pure Fe_2O_3 nanoparticles. The structure of the parent silica remains intact even after loading higher amounts of Fe_2O_3 (see Figure 3S in the Supporting Information. A complete discussion about

[*] Dr. S. Alam, C. Anand, Dr. K. Ariga, Dr. A. Vinu
International Center for Materials Nanoarchitectonics
World Premier International (WPI) Research Center for Materials Nanoarchitectonics (MANA), National Institute for Materials Science
1-1 Namiki, Tsukuba 305-0044, Ibaraki (Japan)
Fax: (+81) 29-860-4706
E-mail: vinu.ajayan@nims.go.jp
Homepage: http://www.nims.go.jp/super/HP/vinu/websitevinu/V-top.htm
Dr. T. Mori
Nano-ionics Materials Group
National Institute for Materials Science
1-1 Namiki, Tsukuba 305-0044, Ibaraki (Japan)
Fax: (+81) 29-860-4663
C. Anand
Department of Chemistry, Anna University, Guindy
Chennai 600025, Tamil Nadu (India)

[**] This work was financially supported Ministry of Education, Culture, Sports, Science and Technology (MEXT) under the Strategic Program for Building an Asian Science and Technology Community Scheme and World Premier International Research Center (WPI) Initiative on Materials Nanoarchitectonics, MEXT, Japan.

Supporting information for this article is available on the WWW under http://dx.doi.org/10.1002/anie.200901570.

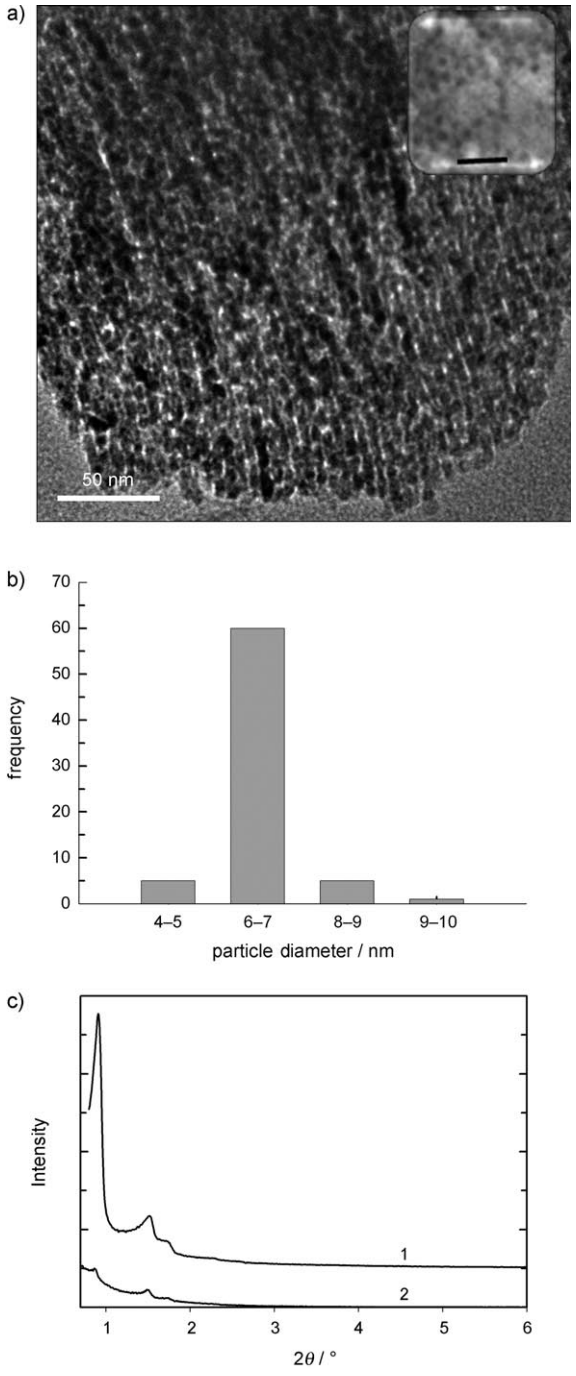

Figure 1. a) Representative HRTEM image of 30F-SBA-15-130. Inset HRSEM image (scale bar = 20 nm). b) Histogram of particle diameter. c) Low-angle regions of the XRD patterns of 1) SBA-15-130 and 2) 30F-SBA-15-130.

particle sizes and phases of iron oxide obtained from the HRTEM image, Brunauer–Emmet–Teller (BET) surface area, and XRD pattern may also be found in the Supporting Information (Figures 2S–7S)).

One of the interesting findings of this work is how the nanocomposite magnetization can be controlled by the pore diameter of the SBA-15 materials. Figure 2a shows the zero-field cooling (ZFC) and field cooling (FC) curves measured at a magnetic field 1000 Oe for Fe_2O_3 nanoparticles grown on

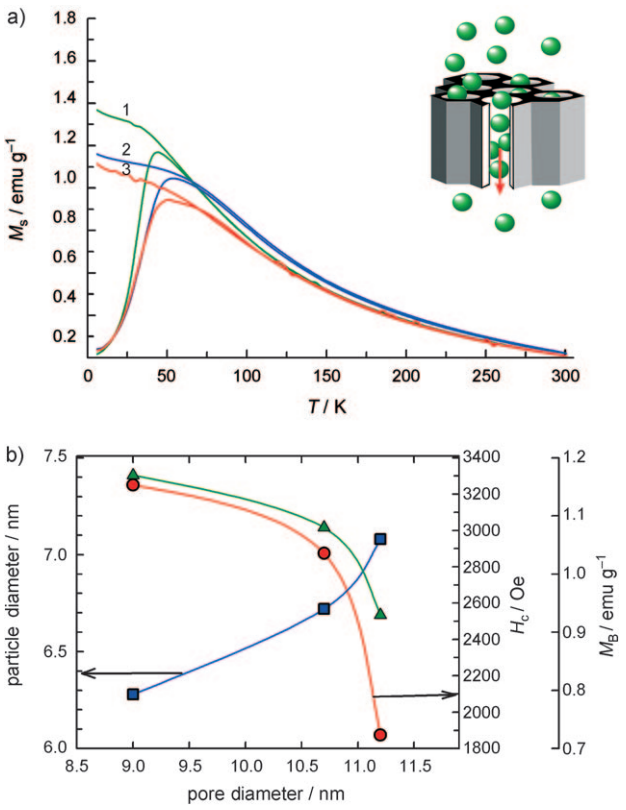

Figure 2. a) FC and ZFC curves of 1) 30F-SBA-15-100, 2) 30F-SBA-15-130, 3) 30F-SBA-15-150. The inset shows a schematic representation of Fe_2O_3 nanoparticles in SBA-15. b) Influence of the template pore diameter on the coercivity H_c and the magnetization at the maxima M_B.

the SBA-15 template with various pore diameters. Interestingly, it can be seen that the blocking temperature T_B is related to the particle size of the Fe_2O_3 nanoparticles (with the assumption that the shape of the particle is spherical) by a simple relation $T_B = KV/25\,k_B$ where K is the anisotropy constant (1.2×10^6 erg cm^{-3}), V is volume of the particle, and k_B is the Boltzmann constant (1.38×10^{-16} erg K^{-1}). The value of T_B increases with the pore diameter of the SBA-15 support. The diameter of the Fe_2O_3 particles prepared using the nanoporous support is calculated to be around 6.3–7.1 nm, which is close to the data obtained from the HRTEM images. Moreover, as the pore diameter of the support decreases, the magnetization and the magnetic coercivity H_c increase with the concomitant decrease of the T_B because of the small particle size (Figure 2 and Tables 1S and 2S in the Supporting Information). This result confirms that the size of the Fe_2O_3 nanoparticles can be controlled by simple adjustment of the pore diameter of the SBA-15 support. It must also be noted that the coercivity and the magnetic remanence vary inversely with the pore diameter of the support and the particle size of the nanoparticles (Figure 2b). To the best of our knowledge, this is the first time that the size of the Fe_2O_3 nanoparticles and their magnetic properties can be tuned by varying the pore diameter of the large-pore mesoporous support SBA-15.

Nanocomposites with different Fe_2O_3 nanoparticle loadings were also prepared and their magnetic properties

studied. Figures 3a and b show the magnetic hysteresis loop measured up to 5 T at 5 K, and the zero field cooling (ZFC) and field cooling (FC) curves measured at 1000 Oe, respectively, for SBA-15-100 with different of Fe_2O_3 nanoparticle

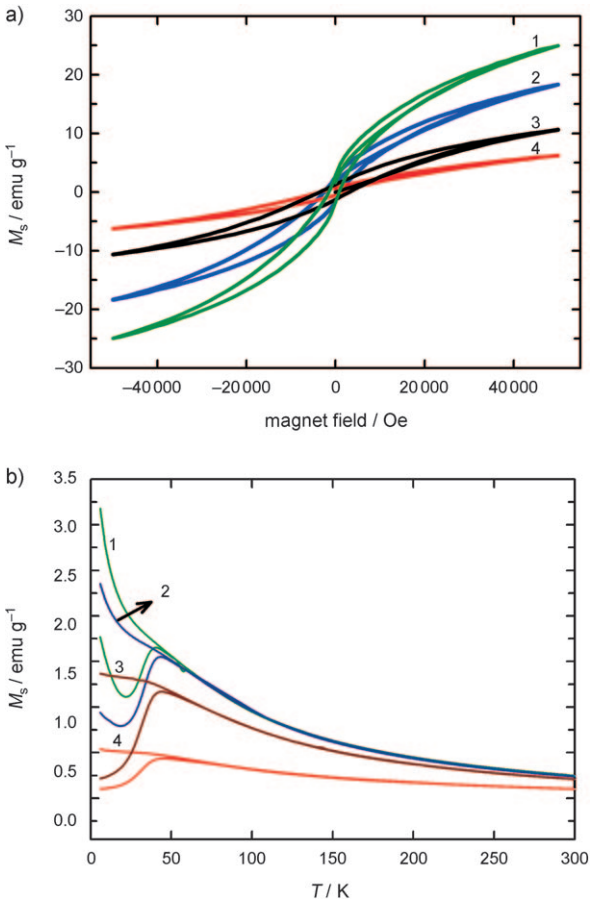

Figure 3. a) Hysteresis and b) ZFC and FC curves: 1) 7.5F-SBA-15-100, 2) 10F-SBA-15-100, 3) 30F-SBA-15-100, and 4) 50F-SBA-15-100.

loadings. The presence of clear hysteresis in the magnetic loops indicates that the Fe_2O_3 nanoparticle encapsulated SBA-15 supports are highly super-paramagnetic, thus confirming a high dispersion of the ultrasmall Fe_2O_3 nanoparticles on the nanoporous surface of the SBA-15 support. It is important to note that the magnetic moments are given per total amount of the Fe on the support. These values are consistent with our previous remarks on the ZFC/FC data of the same samples.

As shown in Figure 3b, a direct correlation between the magnetization and the loading amounts has been clearly observed. The saturation magnetic moment M_s is significantly larger for the sample with a low Fe_2O_3 loading, and decreases as the Fe_2O_3 loading increases. The nanocomposite 7.5F-SBA-15-100 showed the highest M_s of around 25 emu g^{-1}, whereas the nanocomposite with the larger amount of Fe_2O_3, 50F-SBA-15-100, exhibited an M_s of only 6 emu g^{-1}. It is quite obvious that higher amount of Fe_2O_3 nanoparticles inside the nanochannels of SBA-15 enhanced the agglomeration and led to smaller magnetization. It must be also noted that the pore structure of the 50F-SBA-15-100 is almost lost, which is confirmed by the powder XRD pattern, and could also be another reason for the smaller magnetization. Moreover, if the Fe content is higher, then pore blocking will be more likely to occur, thus supporting the formation of large nanoparticles.

On the other hand, the M_s of the pure Fe_2O_3 with the particle size of 53 nm (Figures 1S, 8S, and 9S in the Supporting Information) prepared without the support is approximately 2.1 emu g^{-1}, which is 12 times lower than that of 7.5F-SBA-15-100, thus confirming that the support indeed plays a critical role in controlling the particle size and magnetic properties. Furthermore, it is interesting to note that H_c increases as the Fe loading is increased up to 30 wt%. 30F-SBA-15-100a has an H_c of 3250 Oe, which decreases to 2250 Oe for 50F-SBA-15-100 (Figure 4). These H_c values are much higher than the H_c of 1400 Oe for the Fe_2O_3 nanoparticles prepared without the SBA-15 support. The high H_c of the sample is mainly due to a large screening effect induced by the silica support matrix, and the small Fe_2O_3 nanoparticles in the nanoporous channels.

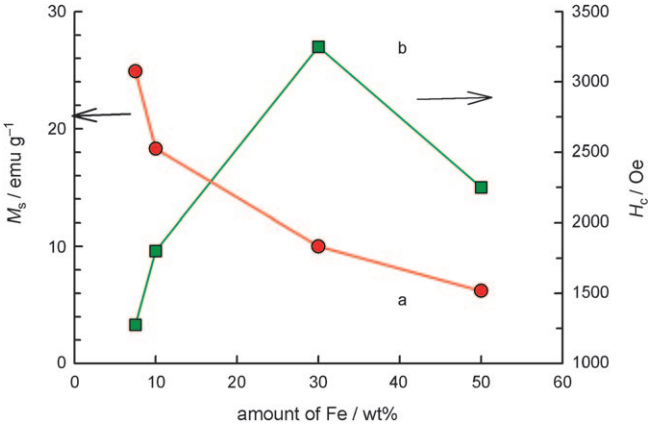

Figure 4. Effect of Fe_2O_3 loading on the magnetic paramters of Fe_2O_3-loaded SBA-15-100: a) M_s and b) H_c values.

In summary, we have demonstrated that Fe_2O_3 nanoparticles can be prepared in a facile nanosieve approach. The nanoparticles are highly dispersed over the SBA-15 support have uniform sizes that can be tuned by simple adjustment of the pore diameter. The size of the nanoparticles is very small, and they show superior magnetic properties compared to the pure Fe_2O_3 nanoparticles prepared without the nanoporous support. These interesting magnetic properties (high M_s and H_c) of the nanocomposites could make them useful for several applications such as magnetic separation and magnetic media. We believe that this method could allow the targeted design and synthesis of various transition metal oxide nanoparticles with different sizes and shapes by using nanoporous silica with three-dimensional structures and tunable pore diameters, such as SBA-16, KIT-6, or SBA-1.

Experimental Section

Preparation of iron oxide nanoparticles over mesoporous supports: Different volumes of a solution of $Fe(NO_3)_3\,9H_2O$ in ethanol (0.5 M) were mixed with the SBA-15 support (100 mg) in ethanol (10 mL). The resulting mixture was stirred at room temperature for 24 h. Subsequently, the ethanol was evaporated by raising the hotplate temperature to 80 °C under stirring. The iron oxide mesoporous nanocomposites were obtained by oxidizing the resulting product in a controlled oxygen flow at 300 °C for 4 h. Characterization of the materials is provided in the Supporting Information.

Received: March 23, 2009
Published online: September 1, 2009

Keywords: iron · magnetic properties · mesoporous supports · nanostructures · silica

[1] a) C. Xu, K. Xu, H. Gu, R. Zheng, H. Liu, X. Zhang, Z. Guo, B. Xu, *J. Am. Chem. Soc.* **2004**, *126*, 9938; b) S. Sun, C. B. Murray, D. Weller, L. Folks, A. Moser, *Science* **2000**, *287*, 1989; c) A.-H. Lu, E. L. Salabas, F. Schuth, *Angew. Chem.* **2007**, *119*, 1242 – 1266; *Angew. Chem. Int. Ed.* **2007**, *46*, 1222 – 1244.

[2] a) J. Bachmann, J. Jing, M. Knez, S. Barth, H. Shen, S. Mathur, U. Gosele, K. Nielsch, *J. Am. Chem. Soc.* **2007**, *129*, 9554; b) J. W. Long, M. S. Logan, C. P. Rhodes, E. E. Carpenter, R. M. Stroud, D. R. Rolison, *J. Am. Chem. Soc.* **2004**, *126*, 16879; c) S. G. Kwon, Y. Piao, J. Park, S. Angappane, Y. Jo, N. M. Hwang, J.-G. Park, T. Hyeon, *J. Am. Chem. Soc.* **2007**, *129*, 12571.

[3] a) T. Hyeon, S. S. Lee, J. Park, Y. Chung, H. B. Na, *J. Am. Chem. Soc.* **2001**, *123*, 12798; b) M. Niederberger, M. H. Bartl, G. D. Stucky, *J. Am. Chem. Soc.* **2002**, *124*, 13642; c) M. Yin, S. J. O'Brien, *J. Am. Chem. Soc.* **2003**, *125*, 6553.

[4] a) C. T. Kresge, M. E. Leonowicz, W. J. Roth, J. C. Vartuli, J. S. Beck, *Nature* **1992**, *359*, 710; b) D. Zhao, J. Feng, Q. Huo, N. Melosh, G. Fredrikson, B. Chmelka, G. D. Stucky, *Science* **1998**, *279*.

[5] M. Hartmann, A. Vinu, *Langmuir* **2002**, *18*, 8010.

